Effect of Aluminum Doping on Performance of HfO_x Based Flexible Resistive Memory Devices

A. D. Paul, S. Biswas, P. Das, H. J. Edwards, V. R. Dhanak, R. Mahapatra, *Member, IEEE*

Abstract— **The Al-doped HfO_x based resistive memory devices have been fabricated on ITO coated PET flexible substrate at room temperature. X-ray photoelectron spectroscopy is used to extract the different doping percentage of Al which allows optimizing the switching performance. It improves the cycle-to-cycle and cell-to-cell uniformity of switching parameters by tuning the oxygen vacancies in HfO_x layers. The 7.5% Al-doped HfO_x based flexible resistive memory device shows excellent switching characteristics such as resistance ratio (>10^3), retention (~10^4 s). There is no degradation of memory window under the mechanical strain with bending radius ranging from 25 mm to 5 mm. The temperature dependent resistive switching characteristics have also been studied. There is sufficient memory window (>10^2) till ~10^4 s at elevated temperature. The I-V curve fitting shows the ohmic (hopping) conduction in LRS and the trap-controlled SCLC in HRS, supported by Arrhenius plot.**

Index Terms— **Al Doping, HfO_x, ReRAM, Flexible**

I. Introduction

Flexible electronics has fascinated much attention for several applications in flexible displays, touch panel devices as well as integrated circuits due to its low cost, low process temperature, light weight, and flexibility [1], [2]. However, the development of flexible memory is one of the key issues for data processing and information storage [3]. The conventional flash memory is hard to be integrated into flexible substrate because of the degraded quality of gate oxide fabricated at low temperature [4], [5]. On the other hand, the resistive random-access memory (ReRAM) [6] has key merits of low process temperature and a simple Metal-Insulator-Metal (MIM) structure for flexible electronics application. But the performance degradation of the flexible substrate-based devices for future memory applications is a major concern [7].

Recently, various metal oxide materials such as TiO_2 [8], Al_2O_3 [9], GO [10], HfO_2 [3], have been studied for the application of flexible ReRAM. Although these metal oxide-based ReRAMs show resistive switching characteristics and flexibility, several issues have to be solved such as low ON/OFF ratio (<10^3), variation of switching parameters [11]. Dispersion in the resistive switching (RS) parameters like SET/RESET voltages, current in Low Resistance State (LRS) and High Resistance state (HRS) is the critical issue of ReRAM. Similar arguments also exist when it comes to flexible ReRAM [12].

In the filament-type ReRAM, the stochastic formation and rupture of the conducting filaments (CFs) causes the variability in the RS properties during switching cycles. Thus, it is essential to effectively control the statistical variation of RS. One of the effective ways is ionic doping in metal oxides to improve the switching stability of the resistive switching [13]. The Ag nanoparticles were embedded in the Al_2O_3/ZnO stack on flexible substrate [14]. It greatly enhanced the device performance, such as high yield and uniformity, low operation voltage and resistance fluctuations. Wang [15] and Zhang et al. [16] showed multi-level memristors based on Si substrate by doping HfO_2 with Cu and Gd, respectively. An improvement in resistive switching properties has been reported in Ni-doped HfO_x [17], Al-doped HfO_x [18]-[20], $HfTiO_x$ [21]. However, most of these traditional ReRAM devices were fabricated on Si substrate at high temperature atomic layer deposition (ALD). The low temperature ALD, plasma enhanced ALD and sputtering techniques can be used for deposition of metal oxides on flexible substrates [3], [22], [23]. However, there is still lacking of reports to study the feasibility and stability of Al-doped HfO_x based ReRAM on flexible substrates. In this work, we have investigated the effect of aluminum (Al) doping on performance of HfO_x based flexible ReRAMs fabricated on ITO coated PET substrate by sputtering system at room temperature. This report is organized as follows: Section II describes device fabrication and characterization methods. The resistive switching characteristics of the fabricated devices including the effect of Al doping on device performance and conduction mechanism have been discussed in Section III. Finally, we conclude the results in Section IV.

II. Experimental

The Al-doped HfO_x based resistive memory devices were fabricated on 130 nm indium tin oxide (ITO) coated flexible polyethylene terephthalate (PET) substrate (≈ 127 μm). The ITO coated PET substrate was first cleaned ultrasonically in acetone, 2-propanol and deionized water. The Al-doped HfO_x thin films of thickness of ≈ 40 nm on PET substrates were deposited by co-sputtering of Hf and

"This work is supported in part by the DST SERB project, Govt of India, Ref no: EMR/2016/006814. ADP acknowledges the UGC NET JRF fellowship for supporting the PhD research work. The authors also acknowledge P. Tiwari for helping to deposit Al at CoE in Advanced Materials" *(Corresponding author: R. Mahapatra.)*

A. D. Paul, S. Biswas, P. Das, R. Mahapatra are with the Department of Electronics and Communication Engineering, National Institute of Technology Durgapur, 713209, India (e-mail: rajat.mahapatra@ece.nitdgp.ac.in).

V. Dhanak, H.J.Edwards are with Department of Physics and Stephenson Institute for Renewable Energy, University of Liverpool, Liverpool L69 7ZF, United Kingdom (e-mail: V.R.Dhanak@liverpool.ac.uk).

Al metal targets using RF and DC sputtering at room temperature varying Ar / O_2 flow ratios (Ar : O_2 = 9:1, 2:1, and 1:1). Then, Al metal dots of diameter in the range of 200-2000 μm were deposited via a hard shadow mask to fabricate Al/Al-doped HfO_x/ITO/PET MIM devices. The schematic and optical image of the final fabricated device is depicted in Fig. 1. An undoped device, Al/HfO_x/ITO/PET was also fabricated for the comparison with the Al-doped samples. The thickness of the Al-doped HfO_x layers was calibrated by spectroscopic ellipsometry measurement of control sample deposited on Si substrate, using a J. A. Wollam VASE ellipsometer with a spectral range of 0.7-5.2 eV at 60-70° in 5° steps. The details of the fabricated MIM devices are given in Table I. The electrical measurement of the devices was carried out using Keysight B2912A source measure unit. The voltages were applied on the top electrode (Al), and the bottom electrode (ITO) was grounded during the electrical measurements. The X-Ray Photoelectron Spectroscopy (XPS) were measured in an ultra-high vacuum system consisting of a twin anode x-ray source and a Scienta SES200 hemispherical electron energy analyser. The XPS spectrometer was calibrated using the Ag $3d_{5/2}$ photoelectron line and the Fermi edge from a clean silver foil first. The spectra were measured in the normal emission geometry with an overall precision of ±0.2 eV. The electron binding energies were corrected using the C 1s peak at 284.8 eV from adventitious surface carbon present in the sputtered films [24]. A Shirley-type background was used for the fitting of all spectra [25]. The measured core level (CL) line-shapes were fitted using a Voigt function to determine the BE position and full width at half maximum (FWHM) of the peaks. The atomic concentration of Al in the Al-doped HfO_x was determined using core level peak area corrected using appropriate atomic sensitivity factors [26].

Table 1: Details of fabricated Al/Al-doped HfO_x/ITO/PET MIM devices

Fabricated Device	Ar:O_2	Aluminium Doping (%)
D1	1:1	3.7%
D2	2:1	7.5%
D3	9:1	9.1%

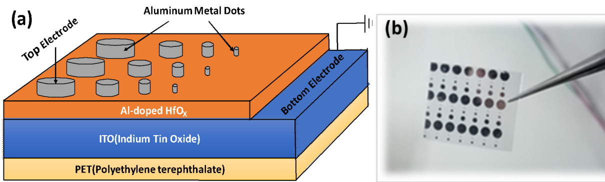

Fig. 1 (a). Schematic diagram of Al/Al-doped HfO_x/ITO/PET for different device sizes. (b) Optical image of Al/ Al-doped HfO_x /ITO/PET fabricated devices with four different device sizes.

III. RESULT AND DISCUSSION

A. Physical characterization:

The XPS core level (CL) spectra of Hf 4d and Al 2p core levels for all Al-doped HfO_x samples are shown in Fig. 2.1. The Al content for sample D1 (Ar : O_2=1:1), D2 (Ar : O_2=2:1) and D3 (Ar : O_2=9:1) are found to be 3.7%, 7.5% and 9.1% respectively. Fig. 2.2 shows XPS of Hf 4f core level (CL) from 3.7% and 7.5% Al-doped HfO_x samples, respectively. The Hf 4f CL has been fitted

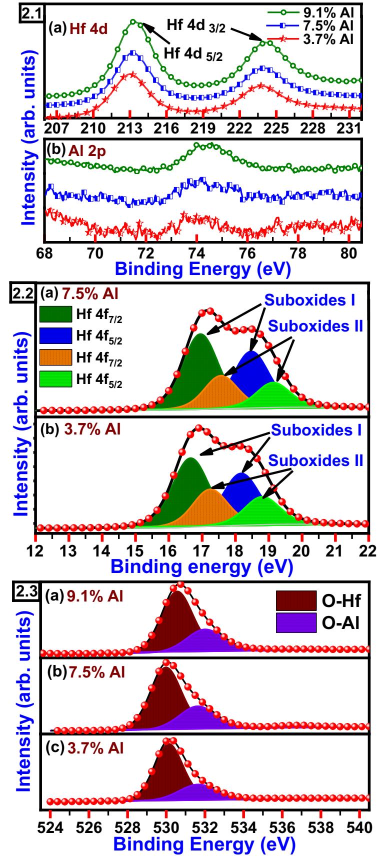

Fig. 2.1 XPS spectra of (a) Hf 4d core level and (b) Al 2p core level for all Al-doped HfO_x samples. Fig 2.2 (a) Hf 4f core level for 7.5% Al-doped HfO_x sample and (b) Hf 4f core level for 3.7% Al-doped HfO_2 sample. Fig 2.3 O 1s core level for (a) 9.1% (b) 7.5% and (c) 3.7% Al-doped HfO_x sample.

with two spin orbit doublets attributed to two different sub oxides. The spin orbit splitting of Hf 4f CL for each sub-oxide is 1.52 eV with an Hf 4f doublet intensity ratio (Hf $4f_{7/2}$: Hf $4f_{5/2}$) of 0.75 as expected. Sub-oxide I is comparatively less stoichiometric than the sub-oxide II, as the Hf $4f_{7/2}$ CL BE value is less in Sub-Oxide I. This implies that the oxygen vacancy (less stoichiometric sub-oxide increasing with increasing Al doping) is also increasing with increasing Al-doping as we are supplying less oxygen with respect to the Ar flow into the sputtering chamber for fabricating higher Al-doped HfO_x samples.

The values of binding energy of different peaks are shown in Table II. With increasing Al doping, the Hf $4f_{7/2}$ peak position (binding energy) and Hf $4f_{7/2}$ peak intensity ratio of sub-oxide I and II increases. Table III shows the binding energies of Hf 4d and Al 2p core levels. Generally all the core level peak positions experience shift to a higher binding energy with the increase of Al doping. This behavior has been observed before and attributed to different charge transfer effects [24], [27].

Table II: Peak position of Hf $4f_{7/2}$ and Hf $4f_{5/2}$ for 3.75% and 7.5% Al-doped HfO_x samples

Sample	Hf $4f_{7/2}$ Sub-Oxide I(eV)	Hf $4f_{5/2}$ Sub-Oxide I (eV)	Hf $4f_{7/2}$ Sub-Oxide II (eV)	Hf $4f_{5/2}$ Sub-Oxide II (eV)
3.7% Al-doped HfO_x	16.65	18.17	17.24	18.80
7.5% Al-doped HfO_x	16.95	18.47	17.57	19.13

Table III: Peak position of Hf $4d_{5/2}$ and Al 2p for 3.7%, 7.5% and 9.1% Al-doped HfO_x samples

Sample	Hf $4d_{5/2}$ (eV)	Al 2p (eV)
3.7% Al-doped HfO_x	212.95	74.01
7.5% Al-doped HfO_x	213.17	74.04
9.1% Al-doped HfO_x	213.32	74.20

Fig. 2.3 shows the O 1s core level for all Al-doped HfOx samples. The O 1s core levels are deconvoluted into two components. The components with lower binding energies (530 eV-530.55 eV) are attributed to the Hf bonded with O whereas the higher binding energy (531.61 eV-531.98 eV) components are attributed to the Al bonded with O. The oxide due to Al appears higher in BE because Al is slightly more electronegative than Hf. The BE values reported are in agreement with literature values [27].

B. DC characterization:

Fig. 3 shows current–voltage (I-V) characteristics of Al-doped HfO_x ReRAM devices of diameter of 200 µm with 9.7%, 7.5% and 3.7% Al doping. In DC voltage sweeping mode, the sequence of bias voltages applied was 0 V → 2 V → 0 V → -5 V → 0 V, and a compliance current of 2 mA was set to safeguard the devices from the hard breakdown of the dielectric. All the devices exhibit typical Bipolar Resistive Switching (BRS) characteristics where the current jumps from high resistance state (HRS) to low resistance state (LRS) in the positive SET voltage and the it reverts back from LRS to HRS at negative RESET voltage. Generally, a higher voltage as compared to SET/RESET voltages is applied to the pristine devices to initiate the switching cycle. Here, no initial separate electroforming process is required to initiate the switching cycle, which could have been due to the pre-existing oxygen vacancies in the Al-doped HfO_x oxides, as observed in XPS analysis.

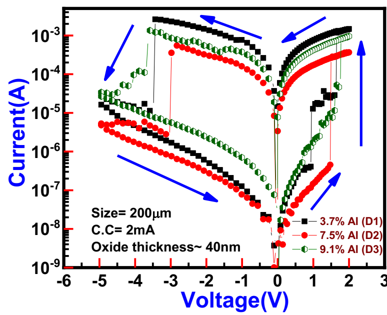

Fig. 3 Current vs. voltage (I–V) characteristics of Al/Al-doped HfO_x/ITO ReRAM with Al doping of 9.1%, 7.5%, and 3.7%. The arrows in the graphs indicate the switching direction.

Fig. 4 presents three box plot distribution of cell-to-cell variation of the SET and RESET voltages (V_{SET} and V_{RESET}), the HRS and LRS currents at 0.1 V (I_{HRS} and I_{LRS}), and the resistance ratio $R_{HRS/LRS}$ at 0.1 V of twenty ReRAMs with different Al doping percentage, respectively. The mean V_{SET} voltages are found to be 1.07 V, 1.40 V, 1.74 V and the mean V_{RESET} voltages are -3.45, -2.85 V and -3.50 V for 3.7%, 7.5% and 9.1% Al doped HfO_x, respectively. However, the 7.5% Al-doped HfO_x shows the minimum cell-to-cell variation of SET and RESET voltages. There is no significant cell-to-cell

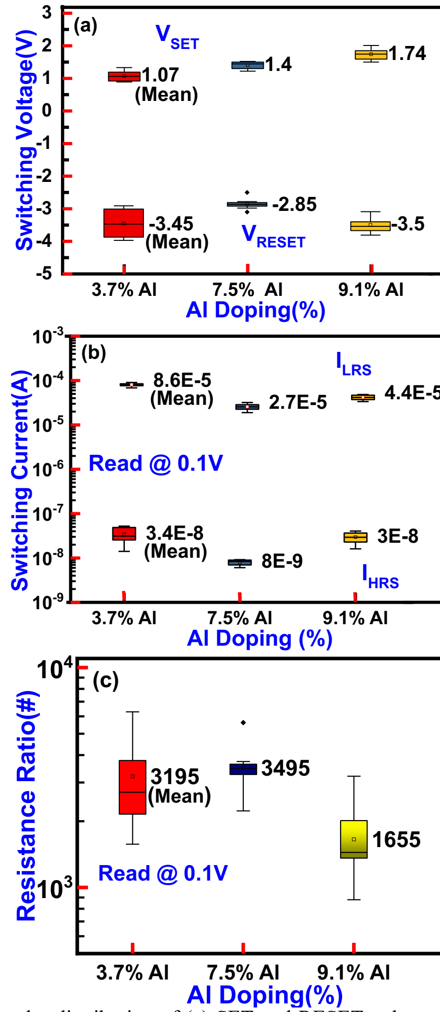

Fig. 4 Box plot distribution of (a) SET and RESET voltages (b) SET and RESET currents and (c) LRS to HRS resistance ratios of Al/Al-doped HfO_x/ITO ReRAMs with different Al doping percentage for twenty different devices. All are read at 0.1 V.

variation of LRS currents of all devices and the variation of HRS current is less for 7.5% Al-doped HfO_x as shown Fig 4(b). The minimum variation of resistance ratio is observed in 7.5% Al-doped HfO_x with the mean value of 3495. The improved resistance ratio has been obtained for Al-doped HfO_x based devices as compared to the extracted value of ≈ 200 [from Fig 5(b)] for undoped HfO_x flexible ReRAM.

Fig 5 represents the cycle-to-cycle cumulative distribution probability of the switching voltages (V_{SET} and V_{RESET}) and HRS and LRS current (I_{HRS} and I_{LRS}) of the device for 7.5% Al-doped HfO_x and undoped HfO_x at room temperature. The I_{HRS} and I_{LRS} currents were measured at 0.1 V. The coefficients of variations of the V_{SET} and V_{RESET} are ≈ 11.60% and ≈ 2.6% for Al-doped HfO_x based devices and the V_{SET} and V_{RESET} for undoped

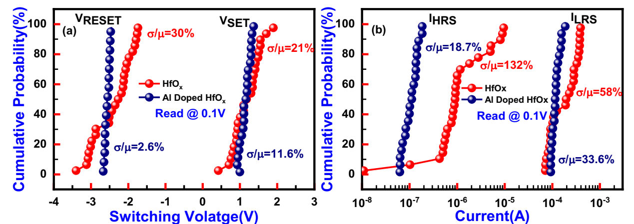

Fig. 5 Probability distribution plots of (a) Switching voltages and (b) Switching currents in HRS and LRS for 7.5% Al-doped HfO_x sample and undoped HfO_x sample (read voltage 0.1 V).

HfO$_x$ based devices are ≈ 21% and ≈ 30% respectively, which indicates that the devices with Al doping (7.5%) maintains excellent uniformity for the reset voltages as well as for set voltages as compared to the undoped HfO$_x$ based devices of 50 repetitive dc sweeps. Similarly, the coefficients of variations of the I_{LRS} and I_{HRS} for 7.5% Al-doped HfO$_x$ are ≈ 33.6% and ≈ 18.7% where as these are increased to ≈ 58% and ≈ 132% for undoped HfO$_x$ devices, respectively.

Although the detailed mechanism of resistive switching in ReRAM remains ambiguous, it is widely accepted that the migration of oxygen vacancies under an applied electrical field plays an important role for the switching behavior [28]. The improved uniform and stable resistive switching behavior in Al-doped HfO$_x$ may be due to Hf-Al-O bonding as observed in XPS analysis. The doping of Al in HfO$_x$ decreases the formation of energy of oxygen vacancies and oxygen vacancies are easily formed near the dopants to improve the switching parameters [19]. The XPS spectra of Hf 4f core levels in Al-doped HfOx thin films (Fig. 2.2) further confirms the presence of non-stoichiometric sub-oxides, which signifies the importance of oxygen vacancies in the resistance switching of ReRAM. However, the different doping percentage of Al modulates the formation of oxygen vacancies and optimizes the switching performance. Similar results have been reported in other study [29].

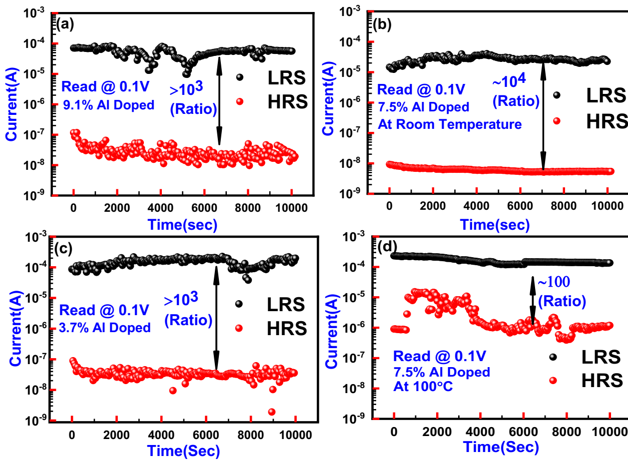

Fig. 6 (a)-(c) Retention characteristic of Al-doped HfO$_x$ ReRAM in LRS and HRS at different Al doping concentration at room temperature. (d) Retention characteristic of 7.5% Al-doped HfO$_x$ ReRAM in LRS and HRS at 100 °C temperature. All the currents are measured at 0.1 V.

Fig. 6 shows the retention characteristics of Al-doped HfO$_x$ flexible ReRAM devices at room temperature and higher temperature. There is no degradation of resistance ratio between LRS and HRS till 10^4 s for all Al-doped devices at room temperature. At the elevated temperature ($100\ ^0$C), the current level in HRS is slightly increased, as shown in Fig. 6 (d). The increased oxygen vacancy related trap density at higher temperature may enhance the temperature-dependent current transport in HRS. However, the sufficient memory margin of ~ 100 still exists till 10^4 s at higher temperature. The excellent retention of the Al-doped HfO$_x$ device is attributed to the presence of Al in constraining the outward diffusion of oxygen vacancies [20].

The flexibility is the key parameter for flexible electronic device applications. The performance of the 7.5% Al-doped HfO$_x$ device under the flexible condition has been investigated for its flexible applications. The resistance of Al/Al-doped HfO$_x$/ITO/PET device in LRS/HRS devices has been measured at the read voltage of 0.1 V with different bending radii starting from the flat condition (20 mm) to the bending condition (5 mm), as shown in Fig. 7. Though, the memory window is slightly decreasing as function of the bending radius, the device shows a stable and sufficient LRS/HRS ratio till the bending up to 5 mm. The decrease of the memory window may be due to the cracks developed in the ITO bottom electrode under extremely flexed condition [3], [30].

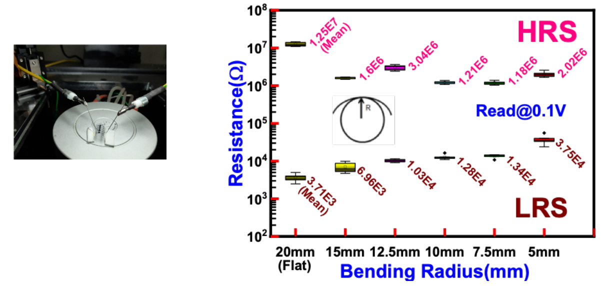

Fig. 7 HRS and LRS resistance plot of Al/Al-doped HfO$_x$/ITO/PET ReRAM under various bending curvature.

Furthermore, we have investigated the conduction mechanism of Al-doped HfO$_x$ devices with different Al percentage. In general, the BRS is likely to be facilitated by electrochemical redox reactions [31]. To understand the conduction and switching mechanisms of the memory device, the I-V characteristics have been replotted in double logarithmic scale of positive as well as negative bias voltages, as shown in Fig. 8. It clearly exhibits that LRS is dominated by ohmic conduction behavior for all Al-doped HfO$_x$ devices with slope ~ 1. The ohmic behaviour in the LRS state has been usually attributed to the formation of CFs in switching oxide layers during the SET process [32]. When a positive voltage is applied to the TE, the oxygen ions (O^{2-}) migrate to the TE, leaving oxygen vacancies. Additionally, the TE Al as an oxygen scavenging layer may enhance the oxygen vacancies in the metal oxide layer [10]. Oxygen vacancies are gathered to form the CFs and the device switches to the LRS. The formation of conductive filament is associated with the presence of oxygen vacancies in switching oxide layers, as observed by the XPS analysis earlier.

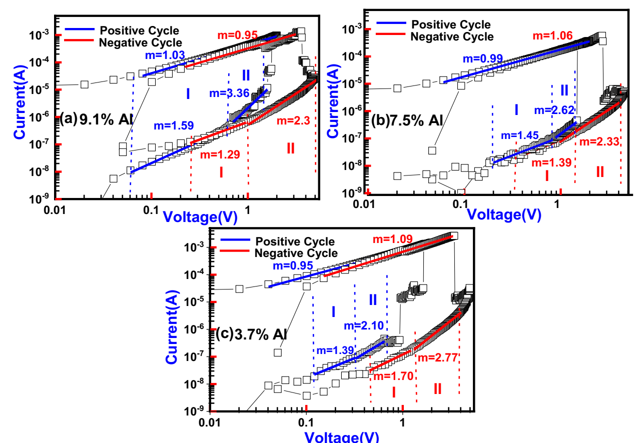

Fig. 8 (a)-(c) Double-logarithmic plot of I-V characteristics of Al/Al-doped HfO$_x$/ITO ReRAM device for positive and negative cycle for 9.1%, 7.5% and 3.7% Al-doping concentration respectively.

However, the conduction mechanism in HRS is much more complicated. The fitted results of I-V curves for HRS in SET cycle consists of an Ohmic region ($I \propto V$) with slope ranging from 1.39 to 1.59 and Child's law region ($I \propto V^2$) with slope ranging from 2.1 to 3.36 for the variation of Al doping from 3.7% to 9.1%, respectively. The slope values in lower voltage region are slightly higher than unity. This may due to the presence of defect related traps in the oxides. This conduction mechanism can be explained in terms of trap-controlled space charge limited conduction (SCLC) [33], where oxygen vacancies present in the Al-doped HfO_x act as traps for the electrons. The variation of slopes with Al doping percentage attributes to the presence of different level of oxygen vacancies created by Al doping. Similarly, fitted I-V curves for HRS in the RESET cycle follows the trap controlled SCLC mechanism.

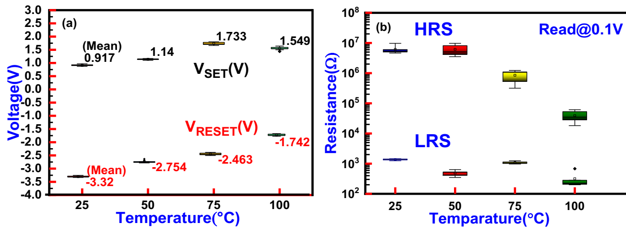

Fig. 9 (a) Box plot distribution of switching voltages with temperature. (b) Box plot distribution of switching resistances with temperature.

To gain a better understanding of the conduction mechanism, the influence of temperature of resistive switching characteristics has been investigated further. Fig. 9 (a) shows the variation of SET and RESET voltages of 7.5% Al-doped HfO_x devices with variation of temperature. The RESET voltages are significantly affected by temperature. It decreases from -3.32 V to -1.74 V with increase of temperature from room temperature to 100 ^{0}C. However, there is lesser increment of SET voltages from 0.91 V to 1.54 V with increase of temperature. Similar observation has been reported in different device structures [32], [34]. The asymmetrical variations of V_{SET} and V_{RESET} with temperature could be attributed to the different temperature dependencies of the SET and RESET processes, which involves oxygen vacancy migration and redox mechanisms [35]. The RESET process is described as a field assisted and temperature activated diffusion process of oxygen ions and vacancies, leading to the rupture of the conducting filament [35], [36]. Therefore, the lower RESET voltage is required at higher temperature to trigger the ionic migration. However, the SET voltage is less dependent on temperature. The effect of temperature is not dominating to form the conductive filament; rather the electric field assists to form the filament by migration of oxygen vacancies. When the temperature increases, there might be a small increase of a parasitic current during the SET process. As a result, a slightly higher SET voltage is required to migrate the oxygen vacancy to form a filament at higher temperature.

The temperature dependence of HRS and LRS resistance is shown in Fig, 9(b). The HRS resistance decreases with increasing in temperature, suggesting a semiconductor like behaviour [37]. As discussed earlier, the carrier transport of the LRS current is followed by ohmic conduction. However, the decrease of LRS

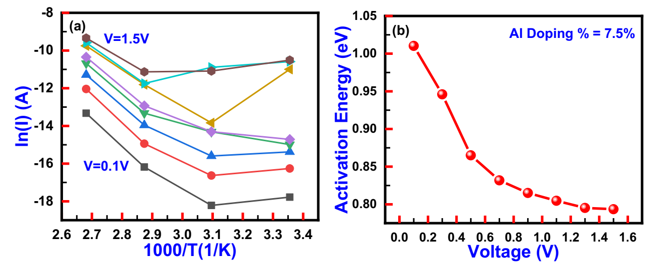

Fig. 10 (a) The ln(I) vs 1000/T curve (Arrhenius plot) of the Al/Al-doped HfO_x/ITO memory devices in HRS at the given voltages with step size 0.2 V. (b) Activation energy as a function of voltage plot for Al/Al-doped HfO_x/ITO devices at HRS.

resistance with increased temperature does not show a clear metallic behavior of the conducting filament. It suggests that the electron transport in LRS may be attributed to electrons hopping among oxygen vacancies which form the conducting filament [38], [39]. This may also suggest the increase of a small parasitic current at higher temperature. Fig. 10(a) demonstrates the Arrhenius plot of HRS current for different bias voltages of the Al/Al-doped HfO_x/ITO/PET device. The Activation Energy (E_a) has been extracted from the slop of the fitted curves. The voltage dependence E_a values are shown in Fig. 10(b). The E_a value is relatively high at low voltage region and it decreases with increase in voltage, which is the characteristic feature of SCLC [37], [40]. Therefore, these temperature-dependent I–V analyses clearly support the SCLC mechanism in HRS.

IV. CONCLUSION

In this article, the switching characteristics and improved uniformity of Al-doped HfO_x based resistive memory devices fabricated at room temperature on flexible substrate have been investigated. The doping of Al in HfO_x tunes the oxygen vacancies which optimize the cycle-to-cycle and cell-to-cell uniformity of switching parameters. The 7.5% Al-doped HfO_x exhibits improved switching characteristics such as resistance ratio (>10^3), retention (~10^4 s). It also maintains the stable resistance ratio under the bending stress for flexible application. The current conduction mechanism is dominated by ohmic (hopping) conduction in LRS and trap-controlled SCLC in HRS.

V. REFERENCES

[1] S.-M. Lee, J. H. Kwon, S. Kwon, and K. C. Choi, "A review of flexible OLEDs toward highly durable unusual displays," IEEE Trans. on Electron Devices, vol. 64, no. 5, pp. 1922-1931, May. 2017, doi: 10.1109/TED.2017.2647964.
[2] A. Lüttgen, S. K. Sharma, D. Zhou, and C. D. Sarris, "Modeling and experimental characterization of flexible touch sensor panels," IEEE Sens. J., vol. 20, no. 5, pp. 2550-2559, Mar. 2020, doi: 10.1109/JSEN.2019.2953586.
[3] J. Shang, W. Xue, Z. Ji, G. Liu, X. Niu, X. Yi, L. Pan, Q. Zhan, X .-H. Xu, and R.-W. Li, "Highly flexible resistive switching memory based on amorphous-nanocrystalline hafnium oxide films," Nanoscale, vol. 9, no. 21, pp. 6939-7306, Feb. 2017, doi: 10.1039/C6NR08687J.
[4] M. T. Ghoneim and M. M. Hussain, "Review on physically flexible nonvolatile memory for internet of everything electronics," Electronics, vol. 4, pp. 424-479, Jul. 2015, doi:10.3390/electronics4030424.
[5] J. S. Meena, S. M. Sze, U. Chand, and T.-Y. Tseng, "Overview of emerging nonvolatile memory technologies," Nanoscale Res. Lett., vol. 9, Sept. 2014, Art. no. 526, doi: 10.1186/1556-276X-9-526.
[6] R. Waser, R. Dittmann, G. Staikov, and K. Szot, "Redox-based resistive switching memories–nanoionic mechanisms, prospects,

and challenges," Adv. Mater., vol. 21, pp. 2632–2663, Jul. 2009, doi: 10.1002/adma.200900375.

[7] C. Dias, D. C. Leitao, C. Freire, H. L. Gomes, S. Cardoso, and J. Ventura, "Resistive switching of silicon-silver thin film devices in flexible substrates," Nanotechnology, vol. 31, Jan. 2020, Art. no. 135702, doi: 10.1088/1361-6528/ab5eb7.

[8] Y. Chen, L. Li, X. Yin, A. Yerramilli, Y. Shen, Y. Song, W. Bian, N. Li, Z. Zhao, W. Qu, N. D. Theodore, and T. L. Alford, "Resistive switching characteristics of flexible TiO_2 thin film fabricated by deep ultraviolet photochemical solution method," IEEE Electron Device Lett., vol. 38, no. 11, pp. 1528-1531, Nov. 2017, doi: 10.1109/LED.2017.2756444.

[9] M. Kim and K. C. Choi, "Transparent and flexible resistive random access memory based on Al_2O_3 film with multilayer electrodes," IEEE Trans. on Electron Devices, vol. 64, no. 8, pp. 3508-3510, Aug. 2017, doi: 10.1109/TED.2017.2716831.

[10] S. K. Hong, J. E. Kim, S. O. Kim, S.-Y. Choi, and B. J. Cho, "Flexible resistive switching memory device based on graphene oxide," IEEE Electron Device Lett.," vol. 31, no. 9, pp. 1005-1007, Sept. 2010, doi: 10.1109/LED.2010.2053695.

[11] S. Yu, X. Guan, and H.-S. P. Wong, "On the switching parameter variation of metal oxide RRAM—part ii: model corroboration and device design strategy," IEEE Trans. on Electron Devices," vol. 59, no. 4, pp. 1183-1188, Apr. 2012, doi: 10.1109/TED.2012.2184544.

[12] X. Cao, Y. Han, J. Zhou, W. Zuo, X. Gao, L. Han, X. Pang, L. Zhang, Y. Liu, and S. Cao, " enhanced switching ratio and long-term stability of flexible RRAM by anchoring polyvinylammonium on perovskite grains," ACS Appl. Mater. Interfaces, vol. 11, pp. 35914-35923, Sept. 2019, doi: 10.1021/acsami.9b12931.

[13] H. Jiang and D. A. Stewart., "Using dopants to tune oxygen vacancy formation in transition metal oxide resistive memory," ACS Appl. Mater. Interfaces, vol. 9, pp. 16296−16304, Apr. 2017, doi: 10.1021/acsami.7b00139.

[14] D.-T. Wang, Y.-W. Dai, J. Xu, L. Chen, Q.-Q. Sun, P. Zhou, P.-F. Wang, S.-J Ding, and D. W. Zhang, "Resistive switching and synaptic behaviors of $TaN/Al_2O_3/ZnO/ITO$ flexible devices with embedded Ag nanoparticles," IEEE Electron Device Lett., vol. 37, no. 7, pp. 878-881, Jul. 2016, doi: 10.1109/LED.2016.2570279.

[15] Y. Wang, Q. Liu, S. Long, W. Wang, Q. Wang, M. Zhang, S. Zhang, Y. Li, Q. Zuo, J. Yang, and M. Liu, "Investigation of resistive switching in Cu-doped HfO_2 thin film for multilevel non-volatile memory applications," Nanotechnology, vol. 21, Jan. 2010, Art. no. 045202, doi: 10.1088/0957-4484/21/4/045202.

[16] H. Zhang, L. Liu, B. Gao, Y. Qiu, X. Liu, J. Lu, R. Han, J. Kang, and B. Yu, "Gd-doping effect on performance of HfO_2 based resistive switching memory devices using implantation approach," Appl. Phys. Lett., vol. 98, Jan. 2011, Art. no. 042105, doi: 10.1063/1.3543837.

[17] T. Tan, Y. Du, A. Cao, Y. Sun, G. Zha, H. Lei, and X. Zheng, "The resistive switching characteristics of Ni-doped HfO_x film and its application as a synapse," J. Alloys Compd., vol. 766, pp. 918-924, Oct. 2018, doi: 10.1016/j.jallcom.2018.07.044.

[18] Y. S. Chen, B. Chen, B. Gao, L. F. Liu, X. Y. Liu, and J. F. Kang, "Well controlled multiple resistive switching states in the Al local doped HfO_2 resistive random access memory device," J. Appl. Phys., vol. 113, no. 16, Apr. 2013, Art. no. 164507, doi: 10.1063/1.4803076.

[19] L. Wu, H. Liu, J. Li, S. Wang, and X. Wang, "A multi-level memristor based on Al-doped HfO_2 thin film," Nanoscale Res. Lett., vol. 14, May. 2019, Art. No. 177, doi: 10.1186/s11671-019-3015-x.

[20] J. Frascaroli, F. Volpe, S. Brivio, and S. Spiga, "Effect of Al doping on the retention behavior of HfO_2 resistive switching memories," Microelectron. Eng., vol. 147, pp. 104-107, Nov. 2015, doi: 10.1016/j.mee.2015.04.043.

[21] B. Chakrabarti, R. V. Galatage, and E. M. Vogel, "Multilevel switching in forming-free resistive memory devices with atomic layer deposited $HfTiO_x$ nanolaminate," IEEE Electron Device Lett., vol. 34, no. 7, pp. 867-869, Jul. 2013, doi: 10.1109/LED.2013.2262917.

[22] R. C. Fang, L. H. Wang, W. Yang, Q. Q. Sun, P. Zhou, P. F. Wang, S. J. Ding, and D. W. Zhang, " Resistive switching of HfO_2 based flexible memories fabricated by low temperature atomic layer deposition," J. Vac. Sci. Technol. B, vol. 30, Apr. 2012, Art. no. 020602, doi: 10.1116/1.3694003.

[23] L. Chen, W. Yang, Y. Li, Q.-Q. Sun, P. Zhou, H.-L. Lu, S.-J. Ding, and D. W. Zhang, "Resistive switching properties of plasma enhanced-ALD La_2O_3 for novel nonvolatile memory application," J. Vac. Sci. Technol. A, vol. 30, no. 1, Jan. 2012, Art. no. 01A148, doi: 10.1116/1.3669516.

[24] P. Ma, J. Sun, G. Zhang, G. Liang, Q. Xin, Y. Li, and A. Song, "Low temperature fabrication of HfAlO alloy dielectric using atomic layer deposition and its application in a low power device," J.Alloys Compd, vol. 792, pp. 543-549, Jul. 2019, doi: 10.1016/j.jallcom.2019.04.015.

[25] D. A. Shirley, "High-resolution X-ray photoemission spectrum of the valence bands of gold," Phys. Rev. B, vol. 5, pp. 4709 –4714, Jun. 1972, doi: 10.1103/PhysRevB.5.4709.

[26] J. F. Moulder, W. F. Stickle, P. E. Sobol, and K. D. Bomben, "Handbook of X-ray photoelectron spectroscopy," Physical Electronics Inc., USA, 1993.

[27] H. Y. Yu, M. F. Li, B. J. Cho, C. C. Yeo, M. S. Joo, D.-L. Kwong, J. S. Pan, C. H. Ang, J. Z. Zheng, and S. Ramanathan, "Energy gap and band alignment for $(HfO_2)_x (Al_2O_3)_{1-x}$ on (100) Si," Appl. Phys. Lett., vol. 81, no. 02, pp. 376-378, Jul. 2002, doi: 10.1063/1.1492024.

[28] S. Maji, S. Samanta, P. Das, S. Maikap, V. R. Dhanak, I. Z. Mitrovic, and R. Mahapatra, "Set compliance current induced resistive memory characteristics of $W/Hf/HfO_x/TiN$ devices," J. Vac. Sci. Technol. B, vol. 37, Apr. 2019, Art. no. 021204, doi: 10.1116/1.5079574.

[29] T. Guo, T. Tan, Z. Liu, and B. Liu, "Oxygen vacancy modulation and enhanced switching behavior in HfO_x film induced by Al doping effect," J. Alloys Compd., vol. 686, pp. 669-674, Nov. 2016, doi: 10.1016/j.jallcom.2016.06.090.

[30] V. K. Nagareddy, M. D. Barnes, F. Zipoli, K. T. Lai, A. M. Alexeev, M. F. Craciun, and C. D. Wright, "multilevel ultrafast flexible nanoscale nonvolatile hybrid graphene oxide-titanium oxide memories," ACS Nano, vol. 11, no. 3, pp. 3010–3021, Feb. 2017, doi: 10.1021/acsnano.6b08668.

[31] K. Baek, S. Park, J. Park, Y.-M. Kim, H. Hwang, and S. H. Oh, "In situ TEM observation on the interface-type resistive switching by electrochemical redox reactions at a TiN/PCMO interface," Nanoscale, vol. 09, pp. 582-593, Nov. 2016, doi: 10.1039/C6NR06293H.

[32] R. Mahapatra, S. Maji, A. B Horsfall, and N. G Wright, "Temperature impact on switching characteristics of resistive memory devices with $HfO_x/TiO_x/HfO_x$ stack dielectric," Microelectron. Eng., vol. 138, no. 20, pp. 118-121, Apr. 2015, doi: 10.1016/j.mee.2015.03.008.

[33] S. Chakrabarti, S. Samanta, S. Maikap, S. Z. Rahaman, and H.-M. Cheng, "Resistive switching characteristics and mechanism using a new $W/WO_3/WO_x/W$ structure", Nanoscale Res. Lett., vol. 11, Sept. 2016, Art. no. 389, doi: 10.1186/s11671-016-1602-7.

[34] C. Walczyk, D. Walczyk, T. Schroeder, T. Bertaud, M. Sowinska, M. Lukosius, M. Fraschke, D. Wolansky, B. Tillack, E. Miranda, and C. Wenger, "Impact of temperature on the resistive switching behavior of embedded HfO_2-based RRAM devices," IEEE Trans. on Electron Devices, vol. 58, no. 9, pp. 3124-3131, Sept. 2011, doi: 10.1109/TED.2011.2160265.

[35] Y. Beilliard, F. Paquette, F. Brousseau, S. Ecoffey, F. Alibart, and D. Drouin, "Investigation of resistive switching and transport mechanisms of Al_2O_3/TiO_{2-x} memristors under cryogenic conditions (1.5K)," AIP Adv., vol. 10, Feb. 2020, Art. no. 025305, doi: 10.1063/1.5140994.

[36] Z. Fang, H. Y. Yu, W. J. Liu, Z. R. Wang, X. A. Tran, B. Gao, and J. F. Kang, "Temperature instability of resistive switching on HfO_x-based RRAM devices," IEEE Electron Device Lett., vol. 31, no. 5, May. 2010, doi: 10.1109/LED.2010.2041893.

[37] X. Zhang, L. Xu, H. Zhang, J. Liu, D. Tan, L. Chen, Z. Ma, and W. Li, "Effect of joule heating on resistive switching characteristic in AlO_x cells made by thermal oxidation formation," Nanoscale Res. Lett., vol. 15, Jan. 2020, Art. no. 11, doi: 10.1186/s11671-019-3229-y.

[38] H. Zhang, B. Gao, B. Sun, G. Chen, L. Zeng, L. Liu, X. Liu, J. Lu, R. Han, J. Kang, and B. Yu, " Ionic doping effect in ZrO_2 resistive switching memory," Appl. Phys. Lett., vol. 96, no. 12, Feb. 2010, Art. no. 123502, doi: 10.1063/1.3364130.

[39] M.–H. Lin, M.–C. Wu, C.–H. Lin, and T.–Y. Tseng, "Effects of vanadium doping on resistive switching characteristics and mechanisms of $SrZrO_3$-based memory films," IEEE Trans. on Electron Devices, vol. 57, no. 8, pp. 1801-1808, Aug. 2010, doi: 10.1109/TED.2010.2050837.

[40] X. L Shao, L. W. Zhou, K. J. Yoon, H. Jiang, J. S. Zhao, K. L. Zhang, S. Yoob, and C. S. Hwang, "Electronic resistance switching in the $Al/TiO_x/Al$ structure for forming-free and area-scalable memory," Nanoscale, vol. 7, May. 2015, Art. no. 11063, doi: 10.1039/c4nr06417h.